Oral exposure to polyethylene microplastics alters gut morphology, immune response, and microbiota composition in mice

Madjid Djouina, Cécile Vignal, Alexandre Dehaut, Ségolène Caboche, Nell Hirt, Christophe Waxin, Charlotte Himber, Delphine Beury, David Hot, Laurent Dubuquoy, et al.

Title page

Title

Oral exposure to polyethylene microplastics alters gut morphology, immune response, and microbiota composition in mice

Author names and affiliations

Madjid DJOUINA[a] Cécile VIGNAL[a], Alexandre DEHAUT[b], Ségolène CABOCHE[c], Nell HIRT[a], Christophe WAXIN[a], Charlotte HIMBER[b], Delphine BEURY[c], David HOT[c], Laurent DUBUQUOY[a], David LAUNAY[a], Guillaume DUFLOS[b], Mathilde BODY-MALAPEL[b]

[a] Univ. Lille, Inserm, CHU Lille, U1286- INFINITE - Institute for Translational Research in Inflammation, F-59000 Lille, France.

[b] ANSES – Laboratoire de Sécurité des Aliments, 6 Boulevard du Bassin Napoléon, 62200 Boulogne-sur-Mer, France.

[c] Univ. Lille, CNRS, Inserm, CHU Lille, Institut Pasteur de Lille, UMR2014 - US41 - PLBS-Plateformes Lilloises de Biologie & Santé, F-59000, Lille, France.

Corresponding author

Mathilde BODY-MALAPEL, PhD

E-mail address

mathilde.body@univ-lille.fr

Full postal address

Institute for Translational Research in Inflammation

INFINITE - Univ. Lille, Inserm, CHU Lille, U1286

Faculté de Médecine - Pôle Recherche,

4éme étage Centre

Place Verdun, F-59045, Lille, Cedex

Abstract

The ubiquitous and growing presence of microplastics (MPs) in all compartments of the environment raises concerns about their possible harmful effects on human health. Human exposure to MPs occurs largely through ingestion. Polyethylene (PE) is widely employed for reusable bags and food packaging and found to be present in drinking water and food. It is also one of the major polymers detected in human stool. The aim of this study was to characterize the effects of intestinal exposure to PE MPs on gut homeostasis. Mice were orally exposed for 6 weeks to PE microbeads of 2 different sizes, 36 and 116 µm, that correspond to those found in human stool. They were administrated either individually or as a mixture at a dose of 100 µg/g of food. Both PE microbead sizes were detected in mouse stool. Different parameters related to major intestinal functions were compared between control mice, mice exposed to each type of microbead, or co-exposed to the 2 types of microbeads. Intestinal disturbances were observed after individual exposure to each size of PE microbead, and the most marked deleterious effects were found in co-exposed mice. At the histomorphological level, crypt depth was increased throughout the intestinal tissues. Significant variations of gene expression related to epithelial, permeability, and inflammatory biomarkers were quantified. Defective recruitment of some intestinal immune cells was observed from the proximal portion of the small intestine to the colon. Several bacterial taxa at the order level were found to be affected by exposure to the MPs by metagenomic analysis of cecal microbiota. These results show that ingestion of PE microbeads induces significant alterations of crucial intestinal markers in mice and underscores the need to further study the health impact of MP exposure in humans.

Keywords

Microplastics. Polyethylene. Mice. Intestinal. Inflammation. Microbiota.

Funding sources

Part of this study was financially supported by the European Union European Regional Development Fund (ERDF), the French State, the French Region Hauts-de-France, and Ifremer, in the framework of the project CPER MARCO 2015-2020.

Introduction

Annual global plastic production has continuously risen since the 1960s and has reached about 368 million tons in 2019 (Plastics Europe, 2021). The total amount of plastic resins and fibers manufactured from 1950 through 2015 is 7800 megatons (Geyer et al., 2017). Poor management in handling of plastic waste has led to a tremendous increase in environmental dumping and ubiquitous spreading of microplastic (MP) contamination (Jambeck et al., 2015; Rillig et al., 2021). MPs are defined as small plastic particles less than 5 mm in size. MPs are purposefully manufactured for various applications, such as exfoliants (microbeads) in personal care products (Wright and Kelly, 2017). This material, along with plastic microfibers from machine-washed clothing, is directly released into the environment through municipal effluent (Wright and Kelly, 2017). MPs present in the environment may also result from fragmentation of larger plastic debris. MPs are detected in freshwater sources as well as tap and bottled water (Danopoulos et al., 2020). They have also been detected in seafood (fish and shellfish), salt, beer, honey, sugar, packaged meats, vegetables, and fruits (Hirt and Body-Malapel, 2020; Kedzierski et al., 2020; Oliveri Conti et al., 2020).

Humans can be exposed to MPs via dermal and inhalational routes, but the risk of exposure by ingestion is of special concern. No epidemiological study has established MP exposure as a causative risk factor for intestinal diseases. However, early experimental studies performed mostly in aquatic organisms showed that exposure to MPs lead to oxidative and inflammatory effects in the intestine and disruption of gut epithelial permeability (Hirt and Body-Malapel, 2020). Regarding polystyrene MP, oxidative stress was described in skeletal muscle, testes, ovaries and liver after oral exposure in mice (Deng et al.,

2017; Li et al., 2021; Shengchen et al., 2021; Wei et al., 2022; Xie et al., 2020). Several studies have shown that polystyrene (PE) MP exposure lead to negative effects on the gut (Jin et al., 2019; Liang et al., 2021; Lu et al., 2018; Luo et al., 2019). For example, a recent study showed that ingestion of PE MPs in mice led to disturbances of gut and serum inflammatory parameters and significant modifications of the intestinal microbiome (B. Li et al., 2020). This may have relevance to societal health since the presence of PE has been detected in human stool (Schwabl et al., 2019; Zhang et al., 2021).

Globally, PE is the most highly produced synthetic, petroleum-based plastic material (Plastics Europe, 2021). PE is extensively used for the manufacture of disposable containers such as bottles and bags (Bardají et al., 2020). Since 1938, PE has widely been applied as a plastic mulch in agriculture (Wang et al., 2019). PE microbeads are also added to cosmetic products, although many countries have banned the sale of rinse-off cosmetics containing MPs (Hunt et al., 2021). As a consequence of this expansive use, inappropriate waste, and insufficient recycling, and also because PE is one of the most resistant polymers to biodegradation, there is a massive accumulation of PE in the environment (Montazer et al., 2020). For example, PE was the most highly abundant plastic polymer found in an Italian river, accounting for 40.5% of total polymers (Munari et al., 2021). PE and polypropylene are the most frequently detected plastic polymers in freshwater and tap water, and the second highest polymer components of MPs in atmospheric fallout (Hirt and Body-Malapel, 2020).

In addition to the large quantities of PE which are accumulating in the environment, PE is also detected in food. For instance, PE was the second most frequent polymer found in edible tissues of shellfish sold for human consumption (Daniel et al., 2021). The widespread use of PE in food packaging for preservation and easy handling purposes during transportation and storage also leads to migration from food packaging to food (Katsara et al., 2021). Consequently, contamination of the environment and food inevitably results in human exposure. Indeed, it has shown that PE, along with polypropylene, polyethylene terephthalate, and polystyrene, are the predominant polymers found in human stool (Schwabl et al., 2019). Moreover, Zhang et al. detected PE in 50% of stool samples collected from Chinese students (Zhang et al., 2021). Noteworthy, the size of MPs detected in human feces ranged from 20 to 800 µm. More recently, human placenta and meconium samples were screened positive for PE

(Braun et al., 2021). Therefore, multiple lines of evidence show that intestinal tissues are in contact with PE MPs.

To further assess the impact of oral PE exposure, mice were exposed for 6 weeks to food spiked with commercial PE microbeads of 2 different average sizes (36 and 116 µm). Mouse stool was analyzed for the presence of the microbeads. Histological analysis and quantification of major parameters of intestinal epithelium were performed to evaluate gut effects. Intestinal immune response was assessed by measurement of cytokine levels and immunophenotyping in small intestine and colon. Finally, composition of the gut microbiome was analyzed by 16S rRNA pyrosequencing.

1. Material and methods

1.1. Particles and chemicals

PE microbeads were acquired from Cospheric (Santa Barbara, USA). Two categories of microbeads were selected, namely red fluorescent beads (Item# UVPMS-BR-1.090 10-45µm) and green fluorescent beads (Item# UVPMS-BG-1.00 106-125µm). The claimed diameter sizes range from 10 to 45 µm for the red beads (RB) and 106 to 125 µm for the green beads (GB).

For chemicals, 10% (w/w) KOH was purchased from Chimie Plus (Vitry-sur-Seine, France), ultra-pure water was acquired from Carlo Erba (Val-de-Reuil, France), and absolute ethanol from VWR (Fontenay-sous-Bois, France).

1.2. Size characterization

An Olympus SZX-16 stereomicroscope equipped with a SDFPLAPO PF 1x/0.15 objective and a UC90 camera was used to capture images by trans-illumination. A magnification of 11.5x was employed for RB and 5x for GB. Microbeads were manually measured using a 3-point circle tool with OlyVIA software (ver. 3.1, build 19668). A total of 312 particles were measured for each category of beads on respectively 5 and 4 fields for RB and GB. Descriptive statistical data were computed using Microsoft Excel.

1.3. Identification of polymeric composition

In order to ascertain the polymeric composition, a microbead of each category was analyzed using a Spotlight™ 400 Fourier-transform infrared (FTIR) spectrometer equipped with a MCT detector coupled to a Spectrum 3 MIR spectrometer. The automatic micro Attenuated Total Reflection (µATR) module was used to acquire spectra. All the recorded spectra were obtained in the transmittance mode in the 4000−600 cm^{-1} region with 2 cm^{-1} resolution and 5 accumulations. Spectra were compared for the 3500–1200 cm^{-1} area to custom reference spectral libraries. Each identification was considered as valid from a score of >0.7.

1.4. Mice and experimental design

All animal procedures were conducted in accordance with the institutional guidelines approved by the institutional Animal Care and Ethical Use Committee of the University of Lille (committee no.75; authorization no. CEEA2017031312157794). C57BL/6 mice were purchased from Janvier Labs (Le Genest-Saint-Isle, France) and housed under standard conditions. Female mice from 7 to 12 weeks old were used in the study. Three independent experiments were performed. Age- and sex-matched mice were used in all experiments. Mice were randomly assigned to 4 experimental groups: 1) control group, receiving control food (final n=9); 2) RB group, receiving food spiked with 100 µg of red PE microbeads/g of food (final n=10); 3) GB group, receiving food spiked with 100 µg of green PE microbeads/g of food (final n=10); and 4) RB+GB group, receiving food spiked with 100 µg of red PE microbeads and 100 µg of green PE microbeads/g of food (final n=10). The intoxication lasted 6 weeks. At necropsy, proximal and distal small intestine, cecum, and colon were sampled.

1.5. Extraction from mouse feces

As a first attempt, mouse feces exposed to both types of microbeads were gently triturated using a tweezer into the bottom of a Petri dish filled with water and observed using an Olympus SZX-16 stereomicroscope with a SDFPLAPO PF 1.6x/0.15 objective.

After feasibility tests, extraction of microbeads from mouse feces was carried out by adapting the method of Dehaut et al., 2016, following the temperature decrease proposed by Treilles et al., 2020

(Dehaut et al., 2016; Treilles et al., 2020). Feces were analyzed individually. For each of the 4 conditions, n=8 feces were weighed on a 0.0001 g sensitivity Sartorius ME215-P analytical balance (Dourdan, France) and placed in a glass beaker. The average mass of feces was 48.1 ± 29.3 mg. After weighing, 10 mL of 10% KOH (m/m) was poured in the beakers and a 2.5 cm magnetic stirrer was added. For digestion, beakers were placed on two multiple stirrers (MIXDrive 6 HT; 2mag, Munich, Germany) with an agitation of 200 rpm for 4 h in a Binder BD 240 incubator (Tüttlingen, Germany) with a temperature of 39.9 ± 1.3°C. Once digested, solutions were filtered with a vacuum system onto a 90 mm GF/A 1.6 µm glass fiber filter set between a VWR 1100 mL funnel and a sintered glass filter holder (Fontenay-sous-Bois, France). The rinsing protocol was carefully performed to increase recovery of the particles on the filter. This protocol consisted of a three-step rinsing using ultra-pure water / 70% (v/v) ethanol / ultra-pure water that was applied on the empty beaker, the empty funnel attached to the filter holder, and a final rinse of the contact area between the funnel and the filter holder.

For a positive control (PC), 10 samples with particles were processed in the same conditions for each batch of digestion. This PC was composed of 10 GB for mice fed with GB, 10 RB for those fed with RB, and 5 GB and 5 RB for mice fed with the mixture of microbeads.

1.6. Histological analysis

At necropsy, tissues were fixed in 4% paraformaldehyde overnight, processed, and embedded in paraffin wax by standard techniques. Serial histological sections of 4 µm thickness were cut, deparaffinized, rehydrated, and stained with Alcian blue and periodic acid-Schiff (AB-PAS). Epithelial area in the colon, villus height, and crypt depth in the proximal and distal small intestine were measured using ImageJ software. For this study, at least 100 well-oriented mucosa, villi, and crypts were measured in at least 5 individual mice from each group. AB-PAS-positive cells were counted under a light microscope (Leica DM5500B).

1.7. Real-time quantitative polymerase chain reaction (PCR)

Small intestinal and colonic tissue samples were homogenized with ceramic beads using Precellys Lysing Equipment (Bertin Technologies, Montigny-le-Bretonneux, France). Total RNA was extracted

with the NucleoSpin RNA kit (Macherey-Nagel, Hoerdt, France). Transcript levels of genes were quantified with the StepOne™ Real-Time PCR system using a SYBR Green PCR master mix (Thermo Fisher Scientific, Villebon-sur-Yvette, France). The primer sequences were designed using Primer Express 3 (Thermo Fisher Scientific) and are available upon request. Melting curve analyses were performed for each sample and gene to confirm the specificity of the amplification. The relative expression of each target gene was normalized to the relative expression of the *Polr2a* gene. Quantification of target gene expression was based on the comparative cycle threshold (Ct) value. The fold changes in the target genes were analyzed by the $2^{-\Delta\Delta Ct}$ method.

1.8. Cell isolation and flow cytometry

At necropsy, the colon and small intestine were harvested and cleaned of fat residue and Peyer's patches for the small intestine. Tissues were open longitudinally, cut into small pieces, and rinsed in cold PBS containing 2% SVF. Pieces were then incubated in predigestion buffer containing EDTA and DTT (Merck KGaA, Darmstadt, Germany) for 30 min at 37°C under agitation. Pieces were then filtered through a 100 µm cell strainer and incubated in digestion solution containing collagenase type 1 (Merck KGaA, Darmstadt, Germany) for 45 min at 37°C under agitation. Cell solution was then passed through a 100 µm cell strainer. Supernatants from the predigestion and digestion steps were then combined and centrifuged. The pellet was resuspended in 44% Percoll (GE Healthcare, Buc, France) and carefully overlaid on a 67% Percoll solution. The Percoll gradient was centrifuged for 20 min and immune cells were recovered from the white ring visible at the interphase of the 2 Percoll solutions. Cells were resuspended in PBS containing a marker of cell viability (Fixable Viability Stain 780; BD Biosciences, Le Pont-de-Claix, France) for 10 min to discriminate viable from non-viable cells in FACS analysis. Cells were then incubated with Fc Block (anti-CD16/CD32; BD Biosciences) for 10 min and then with antibodies in FACS buffer (Brilliant Stain Buffer; BD Biosciences) for 30 min. Antibodies against CD11c (V450; BD Biosciences), CD45 (BV570; Biolegend, San Diego, USA), LY-6G (BV605; BD Biosciences), CD64 (PE; BD Biosciences), I-A/I-E (PE/Dazzle 594; Biolegend), CD11b (BB700; BD Biosciences), CX3CR1 (PE/Cy7; Biolegend), Ly-6C (APC; BD Biosciences), CD4 (PE-Cy7; BD Biosciences), and CD8a (AF532; eBioscience, Thermo Fisher Scientific, Villebon-sur-Yvette, France)

were used along with the isotype control antibodies V450 Hamster IgG1 (BD Biosciences), BV570 Rat IgG2b (Biolegend), BV605 Rat IgG2a (BD Biosciences), PE Mouse IgG1 (BD Biosciences), PE/Dazzle 594 Rat IgG2b (Biolegend), BB700 Rat IgG2a (BD Biosciences), PE/Cy7 Mouse IgG2a (Biolegend), APC Rat IgM (BD biosciences), PE-Cy7 Rat IgG2a (BD Biosciences), and AF532 Rat IgG2a (eBioscience). After washing, cells were analyzed by flow cytometry (Sony SP6800). The generated data were analyzed using FlowJo software (ver. 10.7.1; TreeStar, Stanford, USA).

1.9. Bacterial DNA extraction and Illumina MiSeq sequencing

Genomic DNA was extracted from cecal content using the DNA stool kit (Macherey Nagel, Hoerdt, France). The quantity and purity of DNA (expressed as the ratio of absorbance at 260 and 280 nm) were assessed using a NanoDrop® spectrophotometer (Ozyme, Saint-Cyr-l'Ecole, France). The sequencing library was generated by amplifying the V3-V4 region of the bacterial 16S-rRNA gene using 16S rRNA amplicon generation for MiSeq with the primers Bact-0341 (CCTACGGGNGGCWGCAG) and Bact-0785 (GACTACHVGGGTATCTAATCC). Individual samples were barcoded, pooled to construct the sequencing library, and sequenced using an Illumina MiSeq system (Illumina, San Diego, USA) to generate paired-end 2x300 bp reads.

1.10. Analysis of sequencing data

Bioinformatic analyses were performed using the QIIME2 pipeline (ver. 2020.2) (Bolyen et al., 2019). The Divisive Amplicon Denoising Algorithm 2 (DADA-2) plug-in in QIIME2 was used to filter, dereplicate, identify chimeric sequences, and merge reads to obtain the set of Amplicon Sequence Variants (ASVs) for each sample (Callahan et al., 2016). Then the representative sequences were picked for each ASV. The classify-sklearn plug-in in QIIME2, with the SILVA database (ver. 132), was applied to assign a taxonomic annotation to each representative ASV sequence. In the next step, ASVs identified as eukaryotic contamination (3 ASVs; 12 reads) and external contamination, identified with the decontam package (3 ASVs; 3119 reads), were filtered out (Davis et al., 2018). Diversity metrics (α and β) were obtained with the QIIME2 core-metrics-phylogenetic plug-in, with p-sampling depth parameter fixed to 13781 reads which corresponded to the total frequency that each sample should be rarefied to

prior to computing diversity metrics. This sampling depth allowed retention of >61% of reads and the discarding of only one sample. Tests for differential relative abundance were performed with corncob at the order, family, and genus levels (Martin et al., 2020).

1.11. Statistics

Results are expressed as mean ± standard error of the mean (SEM). The statistical significance of differences between experimental groups was calculated using the Mann-Whitney nonparametric U test (GraphPad Prism software, USA). Statistical significance was defined as $p < 0.05$. For all experiments, * $p<0.05$, ** $p<0.01$, *** $p<0.005$, and **** $p<0.001$ vs control group.

2. Results

2.1. Characterization of microbeads

For size characterization of RB, it was observed that the majority of beads, 94.2%, were included in the size range defined by the supplier (10-45 µm) (Fig. 1A). The percentage was lower for GB, in which only 83.7% of spheres were in the claimed size range (100-125 µm), and 14.1% of particles were lower than 106 µm (Fig. 1B). The median size of spheres was 36 and 116 µm for RB and GB, respectively. This indicates that the size distribution is rather shifted towards the largest particle sizes in the range for each of the bead references. Overall, the size distributions of RB and GB were significantly different (Fig. 1C, $p<0.001$).

Based on observation, the large majority of particles were spherical single chimeric particles for both RB and GB. Some minute polymeric debris, ca. 40, irregular shaped microparticles with size below 10 µm were also observed on the 5 fields of RB.

2.2. Identification of polymeric composition

Based on FITR spectra, the respective top scores obtained for GB and RB were 0.9593 and 0.95889, matching with PE, without signal for other polymers, confirming that microbeads are composed of pure PE polymer (Fig.1D, E)..

2.3. Study of ingested microbeads

2.3.1. Direct observation of mouse feces

During our first attempt to visualize the presence of both sizes of microbeads in mouse stool, both intact and fragmented microbeads were observed (Fig. 1F).

2.3.2. Count and observation after alkaline hydrolysis

Regarding the PCs used during this experiment, different results were obtained depending on the type of beads. Mostly, GB were recovered with acceptable results (Table 1). In one case, 2 beads proved to be fragmented. RB were more difficult to be recovered.

Table 1: Counts of intact and fragmented beads in the positive controls.

	Counts*
Green beads	7/10
Red beads	7/10
Mixture	5/5 (GB)**
	2/5 (RB)

** (GB) Green beads (RB) Red beads*
*** 2 out of the 5 beads were observed as fragments*

For fecal analysis (Table 2), neither GB nor RB was observed in the control mice. For digested feces, observed after exposure of mice to green, red, or a mixture of both types of beads, all samples contained beads except for a single feces of mouse treated with GB.

Table 2 : Count data of intact and fragmented beads observed in the samples (n=8) for the 4 exposure treatments.

	*	Minimum	Maximum	Range	Mean	Std.Error of Mean
Green beads	I	0	5	5	**2.9**	0.69
	F	0	20	20	**4.9**	2.3
Red beads	I	12	135	123	**64**	15
	F	15	88	73	**40**	11
Mixture	IG	1	5	4	**2.8**	0.53
	IR	23	83	60	**46**	7.5
	FG	2	44	42	**17**	5.5
	FR	8	173	165	**55**	19

Controls	I	0	0	0	**0**	0
	F	0	0	0	**0**	0

[*] *I: intact beads, F: fragmented beads, IG: intact green beads, IR: intact red beads, FG: fragmented green beads, FR: fragmented red beads.*

The microbeads were present as both intact and fragmented particles but counts were variable depending on feces, and this heterogeneity was independent of the fecal mass (Table 3). Higher counts were recorded for RB, which was an expected result since food was supplemented with PE MPs based on mass quantities. There was a tendency to have a higher proportion of fragmented GB and intact RB in comparison with their respective counterparts.

Table 3 : Data on oncentrations expressed as number per mg of feces for intact and fragmented beads observed in the samples (n=8) for the 4 exposure treatments.

	[*]	Minimum	Maximum	Range	Mean	Std.Error of Mean
Green beads	I	0.0	0.2	0.2	**0.1**	0.033
	F	0.0	0.5	0.5	**0.15**	0.063
Red beads	I	0.2	2.9	2.7	**1.6**	0.29
	F	0.3	1.7	1.4	**1.0**	0.19
Mixture	IG	0.0	0.2	0.2	**0.088**	0.030
	IR	0.6	3.7	3.1	**1.4**	0.38
	FG	0.1	0.8	0.7	**0.41**	0.11
	FR	0.2	3.8	3.6	**1.4**	0.40
Controls	I	0.0	0.0	0.0	**0.0**	0.0
	F	0.0	0.0	0.0	**0.0**	0.0

[*] *I: intact beads, F: fragmented beads, IG: intact green beads, IR: intact red beads, FG: fragmented green beads, FR: fragmented red beads.*

2.4. Effects of PE microbead exposure on proximal small intestine

After 6 weeks of exposure, weight gain was similar between the 4 groups of mice (112.2±2.8% for CT, 112.3±2.6% for RB, 111.5±1.7% for GB, and 112.6±2.6% for RB+GB, p=0.9 vs CT group). In order to determine if exposure to PE induces morphological alterations of the proximal small intestine, morphometric analyses of this tissue were performed. The measurement of the villus length did not show significant changes in any of the groups (Fig. 2A, B). The crypt depth was increased in the mice exposed to GB (p=0.006) and RB+GB (p=0.002) compared to control mice (Fig. 2A, B). Moreover, the villus/crypt ratio was decreased in the 2 groups of mice exposed to PE individually (p=0.03 for RB and p=0.0006 for GB) and in the group of mice exposed to the mixture of the 2 PE types (p=0.0003; Fig.

293 2C). The AB-PAS-positive area, i.e., the mucin-positive area, was lower in mice exposed to GB
294 (p=0.007) and in mice exposed to RB+GB (p=0.0002; Fig. 2A, D). The transcript levels of the major
295 secretory protein mucin-2 (*Muc2*) was significantly decreased in RB- and GB-exposed mice (p=0.001
296 and p=0.04, respectively; Fig. 2E). Expression levels of major markers of epithelial cell types were also
297 quantified. The absorptive epithelial cell marker villin-1 (*Vil1*) was decreased in RB- and GB-exposed
298 mice (p=0.001 and p= 0.04, respectively; Fig. 2E). The enteroendocrine cell marker chromogranin-A
299 (*Chga*) was downregulated in GB- (p=0.001) and RB+GB-exposed mice (p=0.001; Fig. 2E). The stem
300 cell marker leucine rich repeat containing G protein coupled receptor 5 (*Lgr5*) did not vary (Fig. 2E).
301 The levels of the tight junction-related genes occludin (*Ocln*) and junctional adhesion molecule A (*F11r*)
302 were not modified in PE-exposed mice (Fig. 2F). Assessment of the inflammatory status of the proximal
303 small intestine showed that the mRNA levels of tumor necrosis factor alpha (*Tnf*), interferon gamma
304 (*Ifng*), interleukin-6 (*Il6*), and interleukin-1 beta (*Il1b*) proinflammatory cytokines were not significantly
305 different between the PE-exposed and the control mice (Fig. 2G). Immunophenotyping showed
306 significant variations of the frequency of 4 immune populations: $CD4^+$ T lymphocytes (p=0.03), $CD8^+$
307 T lymphocytes (p=0.03), dendritic cells (p=0.04), and inflammatory monocytes (p=0.004) were
308 reduced in mice exposed to the mixture of the 2 PE microbeads (Fig. 2H).

309 ## 2.5. Effects of PE microbead exposure on distal small intestine

310 For the distal small intestine, an increase of crypt depth was found in RB- (p=0.01) and RB+GB-exposed
311 mice (p=0.003; Fig. 3A, B). The villus/crypt ratio was significantly decreased in the 3 groups of PE-
312 exposed mice (p=0.006, p=0.03, and p<0.0001 for RB, GB, and RB+GB, respectively; Fig. 3C). The
313 mucin area was not significantly modified in any of the PE-exposed groups, as well as *Muc2* transcript
314 expression (Fig. 3A, D, E). In the distal small intestine, a significant increase of *Vil1, Chga,* and *Lgr5*
315 was also measured in RB+GB-exposed mice compared to control mice (p=0.003 for the 3 targets; Fig.
316 3E). *Ocln* and *F11r* mRNA levels tended to decrease in the PE-exposed mice, with a significant decrease
317 of *Ocln* observed in the RB+GB-exposed mice compared to control mice (p=0.04; Fig. 3F).
318 Furthermore, increasing trends of *Tnf*, *Ifng* and *Il1b* were observed in the PE-exposed group, with a
319 significant rise of *Ifng* in GB-exposed mice compared to control mice (p=0.03; Fig. 3G). The levels of

Il6 tended to decrease in PE-exposed mice, with a significant diminution observed in the mice exposed to both PE sizes (p=0.01; Fig. 3G). The frequency of NK cells was increased in distal small intestine of mice exposed to the mixture of PE MPs (p=0.05; Fig. 3H).

2.6. Effects of PE microbead exposure on colon

In colon, the mucosal surface area tended to increase in RB- and GB-exposed mice, and a significant enhancement of the mucosal surface was observed in RB+GB-exposed mice compared to control mice (p=0.03; Fig. 4A, B). The mucin-positive area was also significantly increased in the RB+GB-exposed mice compared to control mice (p=0.003; Fig. 4A, C). Accordingly, *Muc2* mRNA levels were also significantly upregulated between these 2 groups (p=0.0003; Fig. 4D). The expression of *Lgr5* was enhanced in the GB group (p=0.02; Fig4D). The transcripts of *Vil1* and *Chga* were upregulated in colon of GB (p=0.02 and p=0.004, respectively) and RB+GB groups (p=0.001 for both genes; Fig. 4D). These 2 groups also presented a significant overexpression of tight junction-related genes *Ocln* and *F11r* (respectively p=0.001, p=0.002 for GB group and p=0.008, p=0.003 for RB+GB group). For inflammatory cytokines, an upregulation of *Tnf, Ifng, Il6,* and *Il1b* transcripts was observed in the colon of mice exposed to the mixture of PE compared to control mice, although only *Ifng* and *Il6* reached a significant level (p=0.002 for *Ifng*, p=0.005 for *Il6*; Fig. 4F). *Ifng* expression was induced by the exposure to GB MPs (p=0.046). Furthermore, the relative abundance of polynuclear neutrophils was higher in the GB-exposed mice (p=0.02), and the abundance of anti-inflammatory macrophages was lower in both GB- and RB+GB-exposed mice (p=0.05; Fig. 4G).

2.7. Effects of PE microbead exposure on microbiome composition

To assess the impact of PE exposure on the mouse microbiome, V3-V4 amplicons of 16S rRNA genes were sequenced in the cecal content. Exposure to PE did not significantly affect α diversity (Chao1 diversity index; Fig. 5A). The unweighted-UniFrac index showed a significant decrease of β diversity in GB-exposed mice compared to control mice (p=0.02; Fig. 5B). Taxonomic assignment at the phylum level of ASVs, with each color representing an individual bacterial phylum, is shown in Fig. 5C. As expected, *Bacteroidetes* and *Firmicutes* represented the 2 predominant phyla. The effect of PE exposure

was assessed on the abundance of bacterial orders. Several bacteria showed significant changes in relative abundance between the 3 PE-exposed groups and the control group (Fig. 5D). The GB-exposed mice had more abundant Erysipelotrichaceae bacteria (p=0.04). Both RB- and GB-exposed mice had reduced amounts of Verrucomicrobiales (p=0.04 for both groups). By contrast, the relative abundance of Gastranaerophilales was heightened in these 2 PE-exposed groups (p=0.03 for RB- and p=0.04 for GB-exposed mice). An increasing trend for Gastranaerophilale*s* abundance was observed in the RB+GB-exposed group (p=0.06). Lastly, the abundance of Rhodospirillales and Lactobacillales was shown to be increased and decreased, respectively, in RB+GB-exposed mice compared to control mice (p=0.02 for both orders).

Discussion

The aim of this study was to assess whether the presence of PE in intestinal lumen can induce host disturbances. We studied the effects of oral exposure to PE of 2 different average sizes (36 and 116 µm), which present about a 3-fold difference in diameter.These sizes were chosen because they reproduce what has been detected in human feces (Zhang et al., 2021). The concentration of PE was 100 µg/g of food. Assuming the food intake of C57BL/6 mice is 5 g of food/30g body weight (bw)/day, the daily intake of PE was approximately 16.66 mg PE/kg bw/day (Bachmanov et al., 2002). Using the usual interspecies (animal to human) uncertainty factor of 10, this concentration can be extrapolated as 1.66 mg PE/kg bw/day (Dourson et al., 2021). Recently, human ingestion of MPs has been estimated between 0.1 to 5 g weekly, or 0.2 to 10.2 mg/kg bw/day, for a 70 kg adult (Senathirajah et al., 2021). Therefore, the concentration of PE tested was chosen to reflect a realistic human ingestion range of MP. We also tested MP exposure either individually or as a mixture in order to address the issue of potential additive, inhibitory, or synergistic effects.

Our initial analyses confirmed that RB and GB were detected in mouse stool. In the experiment with beads of the positive control, the recovery rate was close to 80% despite the care undertaken to rinse all glassware used for the isolation process with both ultra-pure water and 70% (w/w) ethanol solution. This incomplete recovery may be explained by a stickiness phenomenon resulting from interactions between

glass and the beads. Our analyses also showed a trend of microbead fragmentation in mouse stool. Based on the direct observation of stool without digestion and beads of the positive control, it appears that fragmentation of beads might have occurred during the ingestion and digestion by mice. A second possibility is that fragmentation of microbeads occurred during the extraction process. Indeed, for the latter, we observed in a previous experiment that depending on agitation speeds, microbeads could become fragmented due to the mechanical action of the vortexer and/or possible fragility of the beads.

Exposure to the smaller RB microbeads had no effect in the colon, but induced some significant modifications in proximal and small intestine. The most notable effect of RB exposure was the decrease of villus/crypt ratio both in proximal and distal small intestine. The villus/crypt ratio was also reduced after exposure to GB alone or with the mixture of both MPs. These ultrastructural changes were primarily due to crypt depth enhancement throughout the small intestine and were not associated with villus atrophy, and therefore reflect hypertrophic crypt formation. The hyperproliferation of the crypt compartment can contribute to intestinal tumorigenesis and therefore deserves further investigation (Murray et al., 2021). RB exposure also downregulated mucin-2 and villin-1 gene expression and decreased recruitment of $CD8^+$ T lymphocytes to the proximal small intestine.

The larger microbeads, GB, tended to induce more effects in the intestinal tract than RB. Exposure to GB affected 3 parts of the intestine, with a greater impact on colon. At the histological level, we did not observe any significant difference between GB-exposed mice and control mice, showing that it did not induce severe damage in the colon. Significant disturbances were visible by more sensitive methods such as quantitative RT-PCR and flow cytometry. The proportion of neutrophils and the expression of *Vil1*, *Chga*, *Lgr5*, *Ocln*, *F11r*, and *Ifng* were enhanced, and the recruitment of anti-inflammatory macrophages was impaired in the colon of GB-exposed mice. These results are in concordance with those of Li et al. who found in similar experimental conditions (10-150 µm PE beads, 200µg/g of food, and 5 week exposure) that TLR4, AP-1, and IRF-5 proteins were upregulated in colon, similarly reflecting a proinflammatory state (B. Li et al., 2020). By contrast, Sun et al. showed that oral exposure to smaller PE microbeads (1 to 10µm) at the dosage of 0.2µg/g bw/d decreased Il1β expression, and increased Il8 and Il10 expression, rather in favor of an immunosuppressive effect of PE of this size (Sun

et al., 2021). Therefore, the effects of ingested PE on colonic inflammation appear to be drastically different depending on the size of the microbeads. The difference in effect of RB exposure compared to GB might suggest that even a small difference in particle size at the time of ingestion could influence intestinal toxicity. Consistently, the PS MP uptake into human intestinal epithelial Caco-2 cell line was found greater for 4µm particles than for 1 µm particles (Stock et al., 2019). Furthermore, Sun et al. observed that mouse exposure with PE MPs less than 10 µm in size induced a decreased abundance of Firmicutes and an increased abundance of Bacteroides, whereas these phyla did not vary in our study as well as in the one of Li et al. These findings suggest that the effects of PE MPs on microbiota are also size-dependent, as it has also been observed for PS MPs (Lu et al., 2018)..

The metagenomic analysis of microbiota also revealed that PE microbeads of both sizes individually induced same variations of bacteria abundance at the order level. The Verrucomicrobiales were less abundant and the Gastranaerophilales were more abundant in exposed mice. The role of Verrucomicrobiales is not well known but their increase has been associated with the development of acute colitis in the Dextran Sodium sulfate (DSS)-induced model (Jin et al., 2021; R. Li et al., 2020). Gastranaerophilales are more abundant in DSS-induced colitis (Dou et al., 2020), and follow opposite trends in κ-and ι-carrageenan-induced colitis (Shang et al., 2017). These discrepancies are against an essential effect of these bacterial orders in colonic inflammation.

Another interesting finding is that the most substantial observed changes occurred following exposure to the mixture of the 2 sizes of PE beads. Firstly, we observed an increase of mucosal and mucin areas and an upregulation of *Muc2*, *Vil1,* and *Chga* transcripts in colon reflecting dysregulation of colon mucosa differentiation. An enhancement of *Ocln* and *F11r* expression was also observed suggesting potential barrier dysfunction. The mixture of PE beads induced an increase of *Il6* and *Ifng* expression in favor of a colon proinflammatory state. It also modulated the frequency of $CD4^+$ T lymphocytes, $CD8^+$ T lymphocytes, dendritic cells, and inflammatory monocytes in proximal small intestine, NK cells in distal small intestine, and anti-inflammatory macrophages in colon, showing pronounced alterations of intestinal immune response. Moreover, exposure to the mixture of PE beads decreased the abundance of protective Lactobacillales bacteria (Bartley et al., 2018). Lastly, PE mixture enhanced the frequency

of Rhodospirillales, the increased abundance of which has been associated with several pathological conditions such as Damp Heat syndrome (Jiang et al., 2020), neuropsychiatric symptoms in Alzheimer's disease (Zhou et al., 2021), and animal intoxication with N-nitrosamines (Zhu et al., 2019). Therefore, the imbalance observed in the abundance of Rhodospirillales and Lactobacillales could contribute to the negative effects observed following exposure to the 2 types of microbeads, and this deserves to be further explored. Taken together, these results show that, as a mixture, the 2 sizes of PE microbeads more severely affected the homeostasis of intestinal tissues than as single exposure. Liang et al revealed that in mice, co-exposure to a mixture of PS particles of 50 and 500 nm caused more severe dysfunction of the intestinal barrier than that caused by each PS particles individually (Liang et al., 2021). The authors also demonstrated that co-exposure to several sizes of PS particles modulated their biodistribution in mouse organs and increased their bioavailability. The hypothesis can be put forward that, as for PS, the aggravation of the effects that we observed in the group exposed to RB+GB could be partly explained by an increased bioaccumulation of PE microbeads in the event of co-exposure. Interestingly, in the latter study, exposure 50 nm PS particles increased mucus secretion in the duodenum, jejunum and ileum, whereas it was decreased in the colon. The decline of mucus secretion in colon was confirmed following 0.5, 5 and 50 µm PS MP exposure in mice (Jin et al., 2019; Lu et al., 2018). In our work, mucus secretion was respectively decreased in proximal small intestine and increased in colon after co-exposure to 36 and 116 µm PE MPs, whereas smaller sizes PE MPs reduced colon mucin density (Sun et al. 2021). The comparison of the effects observed on this parameter common to several publications shows that the impact of MPs depends on the type of polymer, its size, and the location in the intestine, which underlines the need to continue testing different experimental conditions in order to allow strong advances in the understanding of the MP toxicological effects.

Taken together, previous and present studies suggest that PE exposure poses a substantial risk to human intestinal health. Moreover, evidence of a positive correlation between the concentration of fecal MPs and the severity of disease activity (Harvey-Bradshaw index and Mayo score) has been recently reported in a cohort of patients with inflammatory bowel disease (IBD) (Yan et al., 2022). Polyethylene was

found in the feces of these patients. Therefore, presence of PE in stool may contribute to the development of inflammation in IBD.

Conclusions

The present study demonstrated that a 6-week oral exposure of mice to PE microbeads induced histological, inflammatory, and immune disturbances from the proximal small intestine to the colon. The relative abundance of bacterial orders was also modified. The co-exposure of 2 sizes of PE microbeads led to defects related to gut differentiation, barrier function, and immune response. These alterations of gut response could contribute in the long term to the onset of immune-mediated inflammatory diseases. Human population studies should be performed to correlate PE exposure levels and disease risks.

CRediT authorship contribution statement

MD: Investigation, CV: Conceptualization, Writing-review, Funding acquisition, AD: Investigation, Methodology, Supervision, Writing-original draft, SC: Formal analysis, NH Investigation, CW: Investigation, CH: Investigation, DB: Investigation, DH: Supervision, LD: Funding acquisition, DL: Funding acquisition, GD: Funding acquisition, Supervision, MB-M: Writing-Original draft, Conceptualization, Validation, Formal analysis, Visualization, Supervision, Revision

Acknowledgments

We thank UMS2014-US41. We would like to thank Nathalie Jouy from the Flow Cytometry Core Facility, BioImaging Center of Lille, for technical advice in flow cytometry. We also thank Thomas Hubert and the staff of the animal facility of Lille, for animal care. We thank Bernadette Leu for her broad-spectrum help. Editorial assistance, in the form of language editing and correction, was provided by XpertScientific Editing and Consulting Services.

Declaration of interest

No conflict of interest to be declared.

References

Bachmanov, A.A., Reed, D.R., Beauchamp, G.K., Tordoff, M.G., 2002. Food Intake, Water Intake, and Drinking Spout Side Preference of 28 Mouse Strains. Behav. Genet. 32, 435–443. https://doi.org/10.1023/A:1020884312053

Bardají, D.K.R., Moretto, J.A.S., Furlan, J.P.R., Stehling, E.G., 2020. A mini-review: current advances in polyethylene biodegradation. World J. Microbiol. Biotechnol. 36, 32. https://doi.org/10.1007/s11274-020-2808-5

Bartley, A., Yang, T., Arocha, R., Malphurs, W.L., Larkin, R., Magee, K.L., Vickroy, T.W., Zubcevic, J., 2018. Increased Abundance of Lactobacillales in the Colon of Beta-Adrenergic Receptor Knock Out Mouse Is Associated With Increased Gut Bacterial Production of Short Chain Fatty Acids and Reduced IL17 Expression in Circulating CD4+ Immune Cells. Front. Physiol. 9, 1593. https://doi.org/10.3389/fphys.2018.01593

Bolyen, E., Rideout, J.R., Dillon, M.R., Bokulich, N.A., Abnet, C.C., Al-Ghalith, G.A., Alexander, H., Alm, E.J., Arumugam, M., Asnicar, F., Bai, Y., Bisanz, J.E., Bittinger, K., Brejnrod, A., Brislawn, C.J., Brown, C.T., Callahan, B.J., Caraballo-Rodríguez, A.M., Chase, J., Cope, E.K., Da Silva, R., Diener, C., Dorrestein, P.C., Douglas, G.M., Durall, D.M., Duvallet, C., Edwardson, C.F., Ernst, M., Estaki, M., Fouquier, J., Gauglitz, J.M., Gibbons, S.M., Gibson, D.L., Gonzalez, A., Gorlick, K., Guo, J., Hillmann, B., Holmes, S., Holste, H., Huttenhower, C., Huttley, G.A., Janssen, S., Jarmusch, A.K., Jiang, L., Kaehler, B.D., Kang, K.B., Keefe, C.R., Keim, P., Kelley, S.T., Knights, D., Koester, I., Kosciolek, T., Kreps, J., Langille, M.G.I., Lee, J., Ley, R., Liu, Y.-X., Loftfield, E., Lozupone, C., Maher, M., Marotz, C., Martin, B.D., McDonald, D., McIver, L.J., Melnik, A.V., Metcalf, J.L., Morgan, S.C., Morton, J.T., Naimey, A.T., Navas-Molina, J.A., Nothias, L.F., Orchanian, S.B., Pearson, T., Peoples, S.L., Petras, D., Preuss, M.L., Pruesse, E., Rasmussen, L.B., Rivers, A., Robeson, M.S., Rosenthal, P., Segata, N., Shaffer, M., Shiffer, A., Sinha, R., Song, S.J., Spear, J.R., Swafford, A.D., Thompson, L.R., Torres, P.J., Trinh, P., Tripathi, A., Turnbaugh, P.J., Ul-Hasan, S., van der Hooft, J.J.J., Vargas, F., Vázquez-Baeza, Y., Vogtmann, E., von Hippel, M., Walters, W., Wan, Y., Wang, M., Warren, J., Weber, K.C., Williamson, C.H.D., Willis, A.D., Xu, Z.Z., Zaneveld, J.R., Zhang, Y., Zhu, Q., Knight, R., Caporaso, J.G., 2019. Reproducible, interactive, scalable and extensible microbiome data science using QIIME 2. Nat. Biotechnol. 37, 852–857. https://doi.org/10.1038/s41587-019-0209-9

Braun, T., Ehrlich, L., Henrich, W., Koeppel, S., Lomako, I., Schwabl, P., Liebmann, B., 2021. Detection of Microplastic in Human Placenta and Meconium in a Clinical Setting. Pharmaceutics 13, 921. https://doi.org/10.3390/pharmaceutics13070921

Callahan, B.J., McMurdie, P.J., Rosen, M.J., Han, A.W., Johnson, A.J.A., Holmes, S.P., 2016. DADA2: High-resolution sample inference from Illumina amplicon data. Nat. Methods 13, 581–583. https://doi.org/10.1038/nmeth.3869

Daniel, D.B., Ashraf, P.M., Thomas, S.N., Thomson, K.T., 2021. Microplastics in the edible tissues of shellfishes sold for human consumption. Chemosphere 264, 128554. https://doi.org/10.1016/j.chemosphere.2020.128554

Danopoulos, E., Twiddy, M., Rotchell, J.M., 2020. Microplastic contamination of drinking water: A systematic review. PloS One 15, e0236838.

Davis, N.M., Proctor, D.M., Holmes, S.P., Relman, D.A., Callahan, B.J., 2018. Simple statistical identification and removal of contaminant sequences in marker-gene and metagenomics data. Microbiome 6, 226. https://doi.org/10.1186/s40168-018-0605-2

Dehaut, A., Cassone, A.-L., Frère, L., Hermabessiere, L., Himber, C., Rinnert, E., Rivière, G., Lambert, C., Soudant, P., Huvet, A., Duflos, G., Paul-Pont, I., 2016. Microplastics in seafood: Benchmark protocol for their extraction and characterization. Environ. Pollut. 215, 223–233. https://doi.org/10.1016/j.envpol.2016.05.018

Deng, Y., Zhang, Y., Lemos, B., Ren, H., 2017. Tissue accumulation of microplastics in mice and biomarker responses suggest widespread health risks of exposure. Sci. Rep. 7, 46687. https://doi.org/10.1038/srep46687

Dou, X., Gao, N., Yan, D., Shan, A., 2020. Sodium Butyrate Alleviates Mouse Colitis by Regulating Gut Microbiota Dysbiosis. Animals 10, 1154. https://doi.org/10.3390/ani10071154

Dourson, M., Ewart, L., Fitzpatrick, S.C., Barros, S.B.M., Mahadevan, B., Hayes, A.W., 2021. The Future of Uncertainty Factors With In Vitro Studies Using Human Cells. Toxicol. Sci. kfab134. https://doi.org/10.1093/toxsci/kfab134

Geyer, R., Jambeck, J.R., Law, K.L., 2017. Production, use, and fate of all plastics ever made. Sci. Adv. https://doi.org/10.1126/sciadv.1700782

Hirt, N., Body-Malapel, M., 2020. Immunotoxicity and intestinal effects of nano-and microplastics: a review of the literature. Part. Fibre Toxicol. 17, 1–22. https://doi.org/10.1186/s12989-020-00387-7

Hunt, C.F., Lin, W.H., Voulvoulis, N., 2021. Evaluating alternatives to plastic microbeads in cosmetics. Nat. Sustain. 4, 366–372.

Jambeck, J.R., Geyer, R., Wilcox, C., Siegler, T.R., Perryman, M., Andrady, A., Narayan, R., Law, K.L., 2015. Plastic waste inputs from land into the ocean. Science 347, 768–771. https://doi.org/10.1126/science.1260352

Jiang, K., Jiang, Q., Mo, X., Li, J., Hu, H., Huang, Q., Guo, W., Qiu, T., Ren, J., Zhang, L., 2020. Study on the Characteristics of Gut Microbiota in Chronic Hepatitis B Patients with Damp Heat Syndrome and Liver Depression and Spleen Deficiency Syndrome.

Jin, M.-Y., Wu, X.-Y., Li, M.-Y., Li, X.-T., Huang, R.-M., Sun, Y.-M., Xu, Z.-L., 2021. Noni (Morinda citrifolia L.) Fruit Polysaccharides Regulated IBD Mice Via Targeting Gut Microbiota: Association of JNK/ERK/NF-κB Signaling Pathways. J. Agric. Food Chem. 69, 10151–10162.

Jin, Y., Lu, L., Tu, W., Luo, T., Fu, Z., 2019. Impacts of polystyrene microplastic on the gut barrier, microbiota and metabolism of mice. Sci. Total Environ. 649, 308–317. https://doi.org/10.1016/j.scitotenv.2018.08.353

Katsara, K., Kenanakis, G., Viskadourakis, Z., Papadakis, V.M., 2021. Polyethylene Migration from Food Packaging on Cheese Detected by Raman and Infrared (ATR/FT-IR) Spectroscopy. Materials 14, 3872. https://doi.org/10.3390/ma14143872

Kedzierski, M., Lechat, B., Sire, O., Le Maguer, G., Le Tilly, V., Bruzaud, S., 2020. Microplastic contamination of packaged meat: Occurrence and associated risks. Food Packag. Shelf Life 24, 100489. https://doi.org/10.1016/j.fpsl.2020.100489

Li, B., Ding, Y., Cheng, X., Sheng, D., Xu, Z., Rong, Q., Wu, Y., Zhao, H., Ji, X., Zhang, Y., 2020. Polyethylene microplastics affect the distribution of gut microbiota and inflammation development in mice. Chemosphere 244, 125492. https://doi.org/10.1016/j.chemosphere.2019.125492

Li, R., Wang, G.P., Whitlock, J.A., Zhao, S., Yagiz, Y., Gu, L., 2020. Muscadine grapes (Vitis rotundifolia) and dealcoholized muscadine wine alleviated symptoms of colitis and protected against dysbiosis in mice exposed to dextran sulfate sodium. J. Funct. Foods 65, 103746. https://doi.org/10.1016/j.jff.2019.103746

Li, S., Ma, Y., Ye, S., Tang, S., Liang, N., Liang, Y., Xiao, F., 2021. Polystyrene microplastics trigger hepatocyte apoptosis and abnormal glycolytic flux via ROS-driven calcium overload. J. Hazard. Mater. 417, 126025.

Liang, B., Zhong, Y., Huang, Y., Lin, X., Liu, J., Lin, L., Hu, M., Jiang, J., Dai, M., Wang, B., Zhang, B., Meng, H., Lelaka, J.J.J., Sui, H., Yang, X., Huang, Z., 2021. Underestimated health risks: polystyrene micro- and nanoplastics jointly induce intestinal barrier dysfunction by ROS-

mediated epithelial cell apoptosis. Part. Fibre Toxicol. 18, 1–19. https://doi.org/10.1186/s12989-021-00414-1
Lu, L., Wan, Z., Luo, T., Fu, Z., Jin, Y., 2018. Polystyrene microplastics induce gut microbiota dysbiosis and hepatic lipid metabolism disorder in mice. Sci. Total Environ. 631–632, 449–458. https://doi.org/10.1016/j.scitotenv.2018.03.051
Luo, T., Wang, C., Pan, Z., Jin, C., Fu, Z., Jin, Y., 2019. Maternal Polystyrene Microplastic Exposure during Gestation and Lactation Altered Metabolic Homeostasis in the Dams and Their F1 and F2 Offspring. Environ. Sci. Technol. 53, 10978–10992. https://doi.org/10.1021/acs.est.9b03191
Martin, B.D., Witten, D., Willis, A.D., 2020. MODELING MICROBIAL ABUNDANCES AND DYSBIOSIS WITH BETA-BINOMIAL REGRESSION. Ann. Appl. Stat. 14, 94–115. https://doi.org/10.1214/19-aoas1283
Montazer, Z., Habibi Najafi, M.B., Levin, D.B., 2020. Challenges with Verifying Microbial Degradation of Polyethylene. Polymers 12, 123. https://doi.org/10.3390/polym12010123
Munari, C., Scoponi, M., Sfriso, A.A., Sfriso, A., Aiello, J., Casoni, E., Mistri, M., 2021. Temporal variation of floatable plastic particles in the largest Italian river, the Po. Mar. Pollut. Bull. 171, 112805. https://doi.org/10.1016/j.marpolbul.2021.112805
Murray, E., Cheng, X., Krishna, A., Jin, X., Ohara, T.E., Stappenbeck, T.S., Bose, R., 2021. HER2 and APC Mutations Promote Altered Crypt-Villus Morphology and Marked Hyperplasia in the Intestinal Epithelium. Cell. Mol. Gastroenterol. Hepatol.
Oliveri Conti, G., Ferrante, M., Banni, M., Favara, C., Nicolosi, I., Cristaldi, A., Fiore, M., Zuccarello, P., 2020. Micro- and nano-plastics in edible fruit and vegetables. The first diet risks assessment for the general population. Environ. Res. 187, 109677. https://doi.org/10.1016/j.envres.2020.109677
Plastics Europe, 2021. Plastics - the Facts 2020 • Plastics Europe. Plast. Eur. URL https://plasticseurope.org/knowledge-hub/plastics-the-facts-2020/ (accessed 1.21.22).
Rillig, M.C., Kim, S.W., Kim, T.-Y., Waldman, W.R., 2021. The Global Plastic Toxicity Debt. Environ. Sci. Technol. 55, 2717–2719. https://doi.org/10.1021/acs.est.0c07781
Schwabl, P., Köppel, S., Königshofer, P., Bucsics, T., Trauner, M., Reiberger, T., Liebmann, B., 2019. Detection of Various Microplastics in Human Stool: A Prospective Case Series. Ann. Intern. Med. https://doi.org/10.7326/M19-0618
Senathirajah, K., Attwood, S., Bhagwat, G., Carbery, M., Wilson, S., Palanisami, T., 2021. Estimation of the mass of microplastics ingested – A pivotal first step towards human health risk assessment. J. Hazard. Mater. 404, 124004. https://doi.org/10.1016/j.jhazmat.2020.124004
Shang, Q., Sun, W., Shan, X., Jiang, H., Cai, C., Hao, J., Li, G., Yu, G., 2017. Carrageenan-induced colitis is associated with decreased population of anti-inflammatory bacterium, Akkermansia muciniphila, in the gut microbiota of C57BL/6J mice. Toxicol. Lett. 279, 87–95. https://doi.org/10.1016/j.toxlet.2017.07.904
Shengchen, W., Jing, L., Yujie, Y., Yue, W., Shiwen, X., 2021. Polystyrene microplastics-induced ROS overproduction disrupts the skeletal muscle regeneration by converting myoblasts into adipocytes. J. Hazard. Mater. 417, 125962.
Stock, V., Böhmert, L., Lisicki, E., Block, R., Cara-Carmona, J., Pack, L.K., Selb, R., Lichtenstein, D., Voss, L., Henderson, C.J., Zabinsky, E., Sieg, H., Braeuning, A., Lampen, A., 2019. Uptake and effects of orally ingested polystyrene microplastic particles in vitro and in vivo. Arch. Toxicol. 93, 1817–1833. https://doi.org/10.1007/s00204-019-02478-7
Sun, H., Chen, N., Yang, X., Xia, Y., Wu, D., 2021. Effects induced by polyethylene microplastics oral exposure on colon mucin release, inflammation, gut microflora composition and metabolism in mice. Ecotoxicol. Environ. Saf. 220, 112340. https://doi.org/10.1016/j.ecoenv.2021.112340
Treilles, R., Cayla, A., Gaspéri, J., Strich, B., Ausset, P., Tassin, B., 2020. Impacts of organic matter digestion protocols on synthetic, artificial and natural raw fibers. Sci. Total Environ. 748, 141230.

Wang, J., Liu, X., Li, Y., Powell, T., Wang, X., Wang, G., Zhang, P., 2019. Microplastics as contaminants in the soil environment: A mini-review. Sci. Total Environ. 691, 848–857. https://doi.org/10.1016/j.scitotenv.2019.07.209
Wei, Z., Wang, Y., Wang, S., Xie, J., Han, Q., Chen, M., 2022. Comparing the effects of polystyrene microplastics exposure on reproduction and fertility in male and female mice. Toxicology 465, 153059. https://doi.org/10.1016/j.tox.2021.153059
Wright, S.L., Kelly, F.J., 2017. Plastic and Human Health: A Micro Issue? Environ. Sci. Technol. 51, 6634–6647. https://doi.org/10.1021/acs.est.7b00423
Xie, X., Deng, T., Duan, J., Xie, J., Yuan, J., Chen, M., 2020. Exposure to polystyrene microplastics causes reproductive toxicity through oxidative stress and activation of the p38 MAPK signaling pathway. Ecotoxicol. Environ. Saf. 190, 110133. https://doi.org/10.1016/j.ecoenv.2019.110133
Yan, Z., Liu, Y., Zhang, T., Zhang, F., Ren, H., Zhang, Y., 2022. Analysis of Microplastics in Human Feces Reveals a Correlation between Fecal Microplastics and Inflammatory Bowel Disease Status. Environ. Sci. Technol. 56, 414–421. https://doi.org/10.1021/acs.est.1c03924
Zhang, N., Li, Y.B., He, H.R., Zhang, J.F., Ma, G.S., 2021. You are what you eat: Microplastics in the feces of young men living in Beijing. Sci. Total Environ. 767, 144345. https://doi.org/10.1016/j.scitotenv.2020.144345
Zhou, Y., Wang, Y., Quan, M., Zhao, H., Jia, J., 2021. Gut Microbiota Changes and Their Correlation with Cognitive and Neuropsychiatric Symptoms in Alzheimer's Disease. J. Alzheimers Dis. JAD 81, 583–595. https://doi.org/10.3233/JAD-201497
Zhu, J., Kong, Y., Yu, J., Shao, S., Mao, M., Zhao, M., Yue, S., 2019. Consumption of drinking water N-Nitrosamines mixture alters gut microbiome and increases the obesity risk in young male rats. Environ. Pollut. 248, 388–396. https://doi.org/10.1016/j.envpol.2019.02.012

Figure captions

Fig. 1. Characterization of polyethylene (PE) microbeads. (A-B) Histograms of size distributions and cumulative percentage of red beads (A) and green beads (B) after measurement of 312 particles for each bead category. (C) The combined density plot. (D-E) FTIR profiles obtained for red bead (D) and green bead (E) from 4,000 to 600 cm^{-1}. For each spectrum the red FTIR profile of PE from a custom library is superimposed. (F) Observation of intact (a) and fragmented (b) green beads and intact (c) and fragmented (d) red beads in mouse stool.

Fig. 2. Effects of polyethylene (PE) exposure on proximal small intestine epithelium histomorphology and immune response. Mice were exposed to food spiked with 100 µg/g of PE microbeads (red beads (RB), green beads (GB), or RB+GB; n=10/group) or control food (CT; n=9) for 6 weeks. (A) Representative pictures of proximal small intestine sections stained with AB-PAS. (B) Villus length and crypt depth. (C) Villus/crypt ratio. (D) Percentage of AB-PAS-positive area. (E) mRNA quantification of markers of intestinal cells *Muc2*, *Vil1*, *Chga*, and *Lgr5*. (F) mRNA quantification of tight junction

genes *Ocln* and *F11r*. (G) mRNA quantification of inflammatory cytokines *Tnf, Ifng, Il6,* and *Il1b.* (H) Percentage of significantly changed immune populations: $CD4^+$ T lymphocytes, $CD8^+$ T lymphocytes, dendritic cells, and inflammatory monocytes. * $p<0.05$ and ** $p<0.01$ vs control group as determined by the Mann-Whitney U test.

Fig. 3. Effects of polyethylene (PE) exposure on distal small intestine epithelium histomorphology and immune response. Mice were exposed to food spiked with 100 µg/g of PE microbeads (red beads (RB), green beads (GB), or RB+GB; n=10/group) or control food (CT; n=9) for 6 weeks. (A) Representative pictures of distal small intestine sections stained with AB-PAS. (B) Villus length and crypt depth. (C) Villus/crypt ratio. (D) Percentage of AB-PAS-positive area. (E) mRNA quantification of markers of intestinal cells *Muc2*, *Vil1, Chga,* and *Lgr5*. (F) mRNA quantification of tight junction genes *Ocln* and *F11r*. (G) mRNA quantification of inflammatory cytokines *Tnf, Ifng, Il6*, and *Il1b.* (H) Percentage of the significantly changed immune population of NK cells. * $p<0.05$, ** $p<0.01$, *** $p<0.005$, and **** $p<0.001$ vs control group as determined by the Mann-Whitney U test.

Fig. 4. Effects of polyethylene (PE) exposure on colon epithelium histomorphology and immune response. Mice were exposed to food contaminated with 100 µg/g of PE microbeads (red beads (RB), green beads (GB), or RB+GB; n=10/group) or control food (CT; n=9) for 6 weeks. (A) Representative pictures of colon sections stained with AB-PAS. (B) Mucosal surface area. (C) Percentage of AB-PAS-positive area. (D) mRNA quantification of markers of intestinal cells *Muc2, Vil1, Chga*, and *Lgr5*. (E) mRNA quantification of tight junction genes *Ocln* and *F11r*. (F) mRNA quantification of inflammatory cytokines *Tnf, Ifng, Il6*, and *Il1b.* (G) Percentage of significantly changed immune populations: polymorphonuclear neutrophils and anti-inflammatory macrophages. * $p<0.05$, ** $p<001$, and *** $p<0.005$ vs control group as determined by the Mann-Whitney U test.

Fig. 5. Effects of polyethylene (PE) exposure on the gut microbiome. Mice were exposed to food spiked with 100 µg/g of PE microbeads (red beads (RB), green beads (GB), or RB+GB; n=7-8/group) or control food (CT; n=7) for 6 weeks. (A) Chao1 α diversity index. (B) Unweighted UniFrac β diversity index; * $p<0.05$ as determined by pairwise PERMANOVA. (C) Overview of the relative abundance of gut

686 bacteria depicted at the phylum level. (D) Differential abundance of significantly changed bacterial
687 orders. * $p<0.05$ vs control group as determined by Corncob test.

688

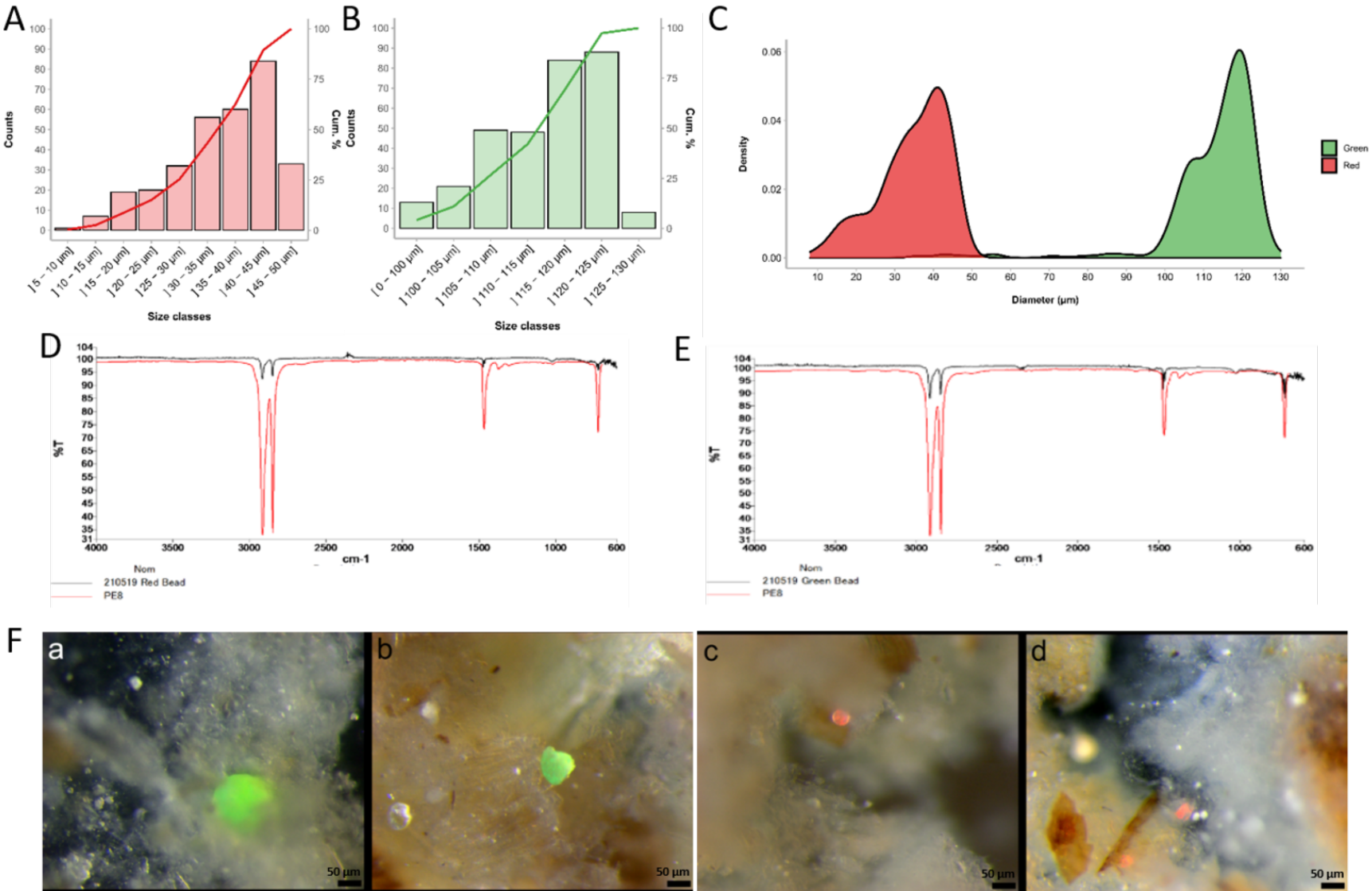
A
Counts
Cum. %
Size classes
]5 – 10 µm]
]10 – 15 µm]
]15 – 20 µm]
]20 – 25 µm]
]25 – 30 µm]
]30 – 35 µm]
]35 – 40 µm]
]40 – 45 µm]
]45 – 50 µm]
B
Counts
Cum. %
Size classes
[0 – 100 µm]
]100 – 105 µm]
]105 – 110 µm]
]110 – 115 µm]
]115 – 120 µm]
]120 – 125 µm]
]125 – 130 µm]
C
Density
Diameter (µm)
Green
Red
D
%T
cm-1
Nom
210519 Red Bead
PE8
E
%T
cm-1
Nom
210519 Green Bead
PE8
F
a
b
c
d
50 µm

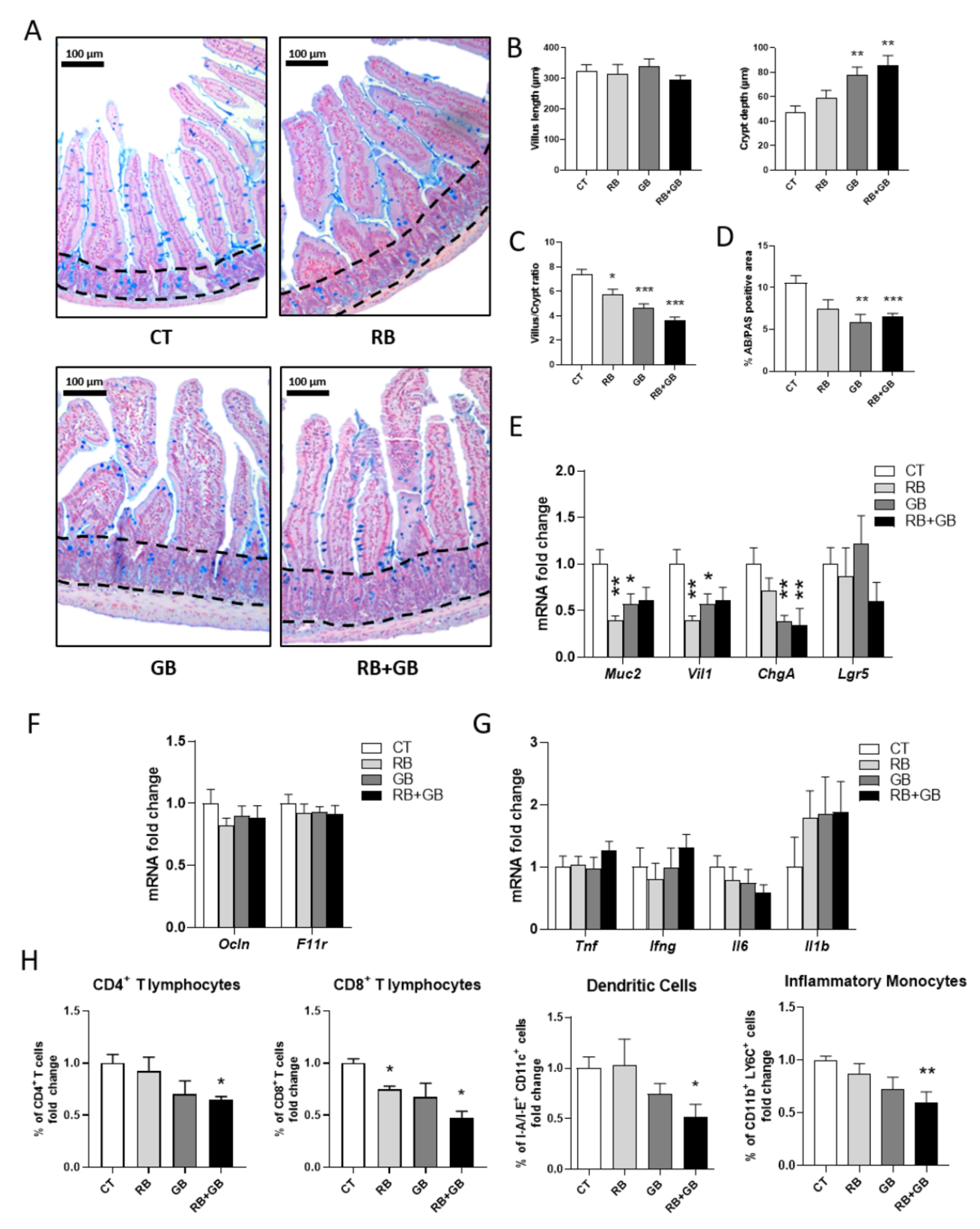
A
100 µm
CT
RB
GB
RB+GB
B
Villus length (µm)
Crypt depth (µm)
C
Villus/Crypt ratio
D
% AB/PAS positive area
E
mRNA fold change
Muc2
Vil1
ChgA
Lgr5
F
Ocln
F11r
G
Tnf
Ifng
Il6
Il1b
H
CD4+ T lymphocytes
CD8+ T lymphocytes
Dendritic Cells
Inflammatory Monocytes

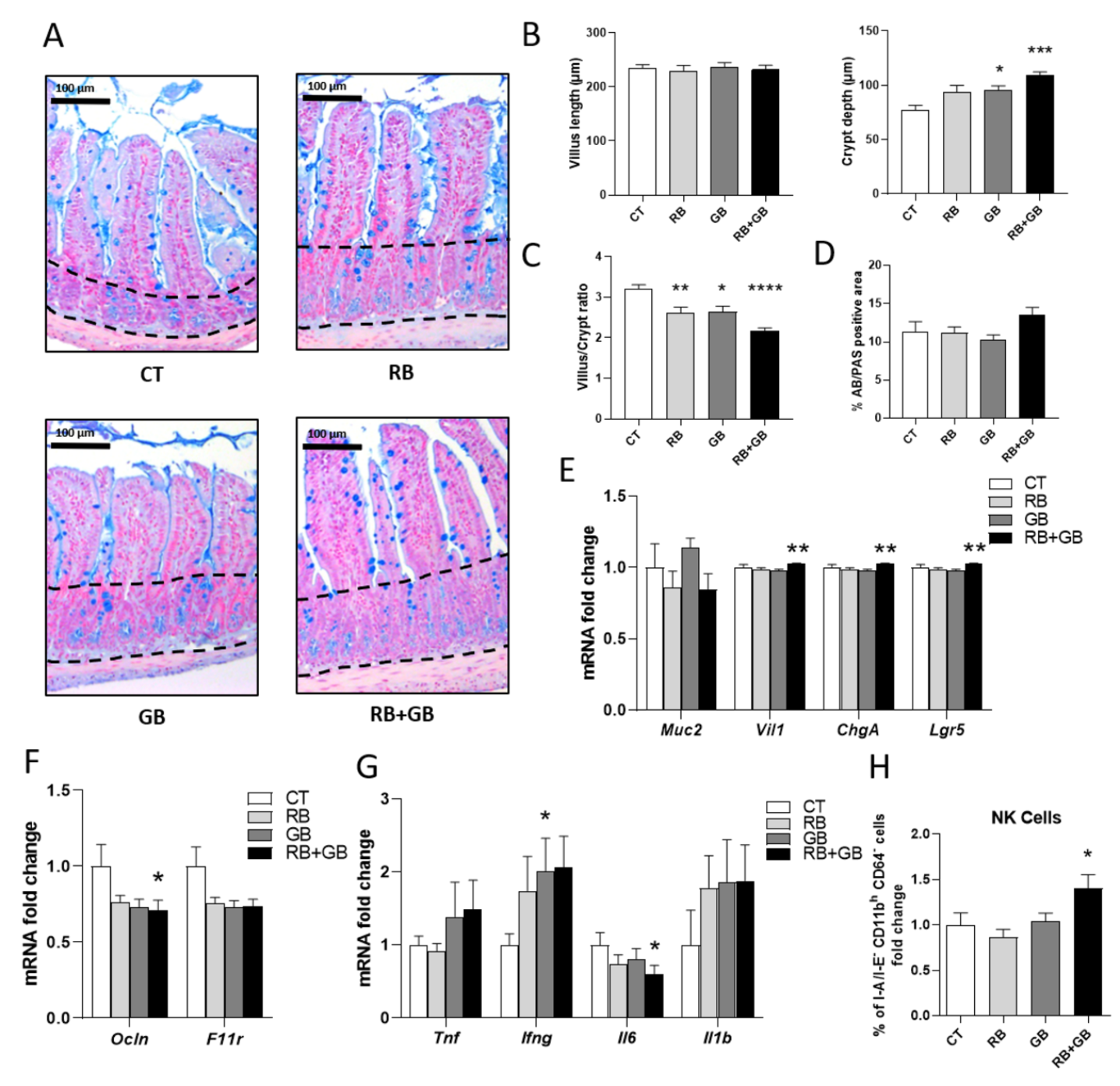
A
100 µm
CT
RB
GB
RB+GB
B
Villus length (µm)
Crypt depth (µm)
C
Villus/Crypt ratio
D
% AB/PAS positive area
E
mRNA fold change
Muc2
Vil1
ChgA
Lgr5
F
Ocln
F11r
G
Tnf
Ifng
Il6
Il1b
H
NK Cells
% of I-A/I-E- CD11b^h CD64- cells fold change

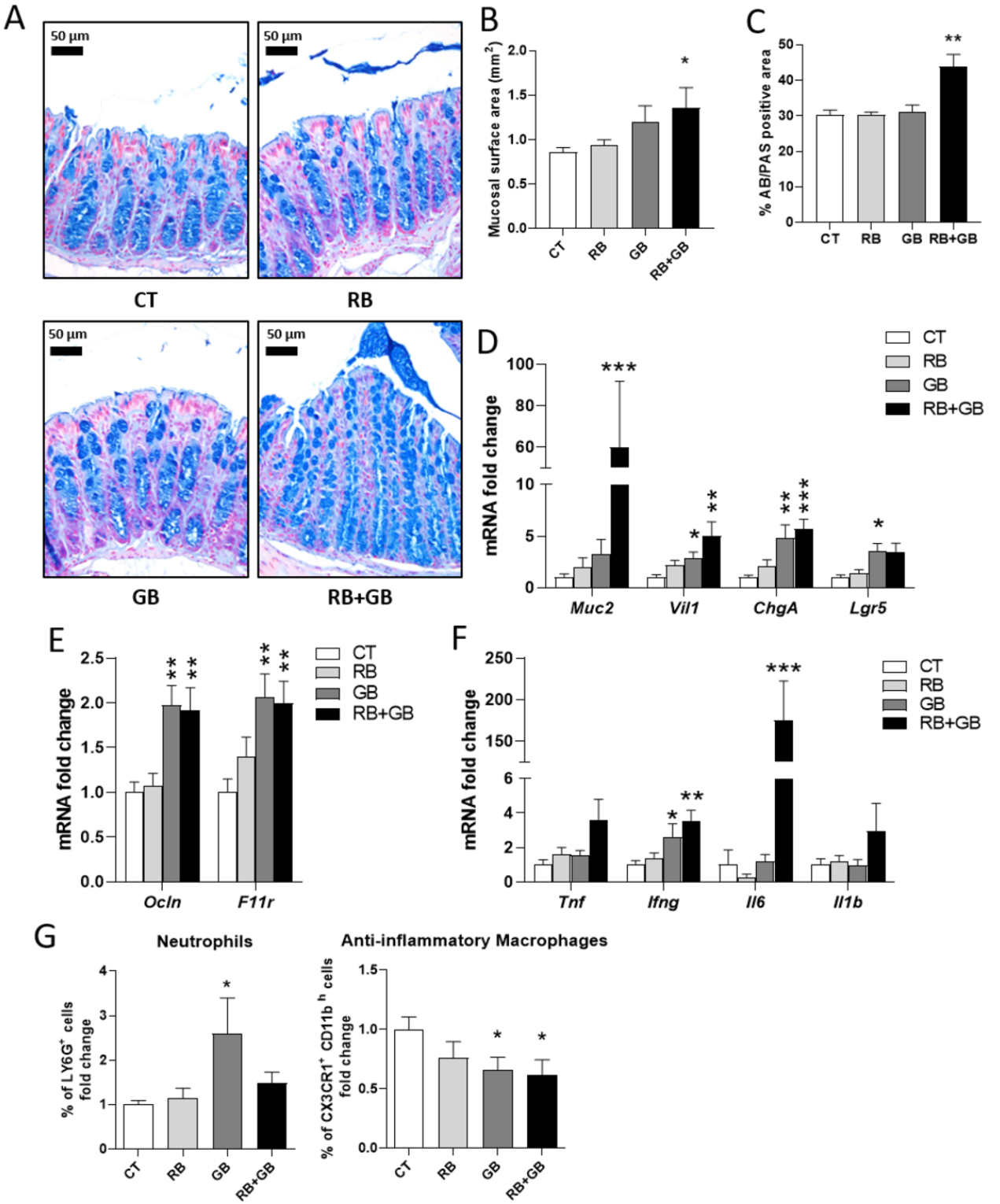
A
50 µm
CT
RB
GB
RB+GB
B
Mucosal surface area (mm²)
C
% AB/PAS positive area
D
mRNA fold change
Muc2
Vil1
ChgA
Lgr5
E
Ocln
F11r
F
Tnf
Ifng
Il6
Il1b
G
Neutrophils
% of LY6G⁺ cells fold change
Anti-inflammatory Macrophages
% of CX3CR1⁺ CD11b ʰ cells fold change

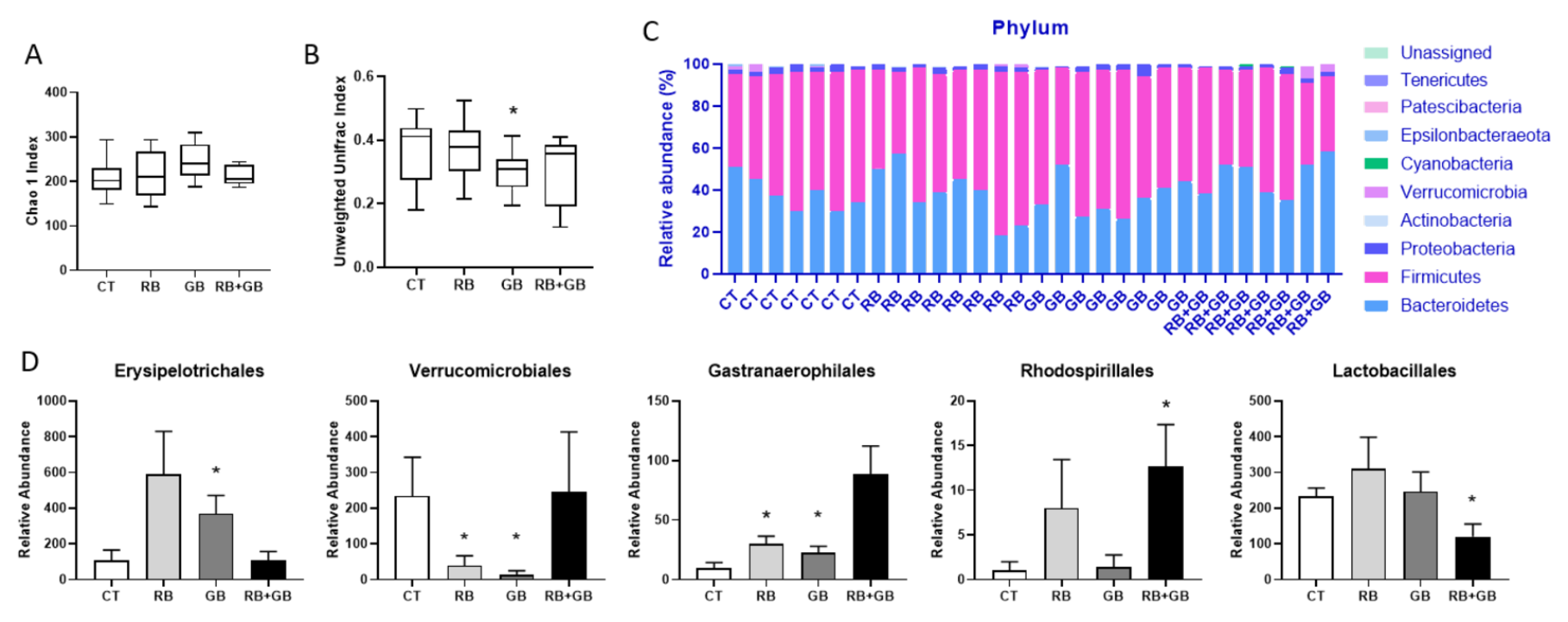
A
Chao 1 Index
400
300
200
100
0
CT
RB
GB
RB+GB
B
Unweighted Unifrac Index
0.6
0.4
0.2
0.0
*
CT
RB
GB
RB+GB
C
Phylum
Relative abundance (%)
100
80
60
40
20
0
CT CT CT CT CT CT CT RB RB RB RB RB RB RB RB GB GB GB GB GB GB GB RB+GB RB+GB RB+GB RB+GB RB+GB RB+GB RB+GB
Unassigned
Tenericutes
Patescibacteria
Epsilonbacteraeota
Cyanobacteria
Verrucomicrobia
Actinobacteria
Proteobacteria
Firmicutes
Bacteroidetes
D
Erysipelotrichales
Relative Abundance
1000
800
600
400
200
0
*
CT
RB
GB
RB+GB
Verrucomicrobiales
Relative Abundance
500
400
300
200
100
0
* *
CT
RB
GB
RB+GB
Gastranaerophilales
Relative Abundance
150
100
50
0
* *
CT
RB
GB
RB+GB
Rhodospirillales
Relative Abundance
20
15
10
5
0
*
CT
RB
GB
RB+GB
Lactobacillales
Relative Abundance
500
400
300
200
100
0
*
CT
RB
GB
RB+GB